http://dx.doi.org/10.5012/bkcs.2014.35.11.3227

Bamboo-like Te Nanotubes with Tailored Dimensions Synthesized from Segmental NiFe Nanowires as Sacrificial Templates

Hoyoung Suh, Hyun Sung Jung,[†,‡] Nosang V. Myung,[†] and Kimin Hong[*]

Department of Physics, Chungnam National University, Daejeon 305-764, Korea. [*]E-mail: kmhong@cnu.ac.kr
[†]Department of Chemical and Environmental Engineering, University of California-Riverside, Riverside, CA 92521, USA
[‡]Advanced Materials Convergence Division, Korea Institute of Ceramic Engineering & Technology, Seoul 153-801, Korea
Received June 11, 2014, Accepted July 15, 2014

Bamboo-like Te nanotubes were synthesized *via* the galvanic displacement reaction of NiFe nanowires with Ni-rich and Fe-rich segments. The thick and thin components of the synthesized Te nanotubes were converted from the Ni-rich and Fe-rich segments in the NiFe nanowires respectively. The dimensions of the Te nanotubes were controlled by employing sacrificial NiFe nanowires with tailored dimensions as the template for the galvanic displacement reaction. The segment lengths of the Te nanotubes were found to be dependent on those of the sacrificial NiFe nanowires. The galvanic displacement reaction was characterized by analyzing the open circuit potential and the corrosion resistance.

Key Words : Galvanic displacement reaction, Bamboo-like Te nanotube, Segmental NiFe nanowire, Overpotential deposition

Introduction

With recent advances in nanotechnology, the fabrication of one-dimensional (1-D) nanostructures has become an attractive approach to enhancing the performances of nano-devices. 1-D nanostructure-based nano-devices have diverse functionalities in devices and interconnectors because of their high surface to volume ratios, the quantum size effects of their tailored dimensions, and low power consumption.[1-5] Recently, a new approach to the fabrication of 1-D hetero-structures such as nanopeapods, core-shell nanowires, multi-segmental nanowires, and dumbbell-like nanowires has been developed that expands the range of properties and functionalities of 1-D nanostructures.[6-11]

Conventional physical and chemical depositions have mainly been utilized in the synthesis of 1-D nanostructures with well-controlled morphologies and dimensions.[12-17] However, it is difficult to use vapor deposition techniques for the synthesis of 1-D nanostructures with complex hetero-nanostructures and tailored dimensions. The galvanic displacement reaction (GDR) of a template consisting of electro-deposited heterostructures is a powerful and cost-effective technique for the creation of complex heterostructures in a wide range of materials with controllable dimensions, compositions, and morphologies. GDR is a spontaneous electro-chemical reaction driven by the difference between the redox potentials of the sacrificial material and the ions in the electrolyte at nearly ambient conditions without the aid of an external power source.[7-10,18-25]

Tellurium is a p-type semiconductor with a narrow band gap of 0.35 eV at room temperature. 1-D Te nanostructures have been found to exhibit excellent properties in electrical and optical devices such as room temperature gas sensors, thermoelectric devices, piezoelectric devices, and photo-conductors. Such nanostructures have been synthesized with various techniques: physical/chemical vapor deposition, solvo-thermal/hydrothermal reactions, template-directed electro-deposition, and microwave-assisted reactions.[15-17,26-29] Recent-ly, there have been attempts to synthesize various 1-D Te nanostructures *via* the GDRs of sacrificial materials such as metallic thin films and nanofibers.[23,25,30]

In this study, we first electroplated 1-D NiFe nanowires for use as sacrificial materials. We then applied the GDR process to the NiFe nanowires to obtain Te nanostructures. 1-D Te nanostructures with tailored heterostructures were synthesized by tuning the dimensions and composition of sacrificial metal nanowires and in particular the dimensions and compositions of their segments. The diameter and seg-ment length of the synthesized bamboo-like Te nanotubes were controlled by employing sacrificial metal nanowires with tailored dimensions. The conversion of the segmental metal nanowires to heterostructured Te nanotubes *via* a GDR was characterized by examining the evolution of the surface morphologies during the reaction and performing electrochemical analysis.

Experimental

Commercially available AAO (Anodized Aluminum Oxide) membranes with a nominal pore diameter of 200 nm (Whatman Inc.) and track-etched polycarbonate membranes (Whatman Inc.) with a nominal pore diameter of 100 nm were utilized as templates to synthesize nanowires with various diameters. Segmental NiFe nanowires with Ni-rich and Fe-rich components were prepared by electrodeposition method utilizing porous AAO membranes for use as a sacri-ficial material.[9,22] The length of each segment was controlled by varying the plating time. The plating electrolyte was

composed of 0.9 M $FeCl_2$, 0.6 M $NiCl_2$, 1.0 M $CaCl_2$, and 0.03 M L-ascorbic acid in deionized water with adjusted pH of 0.7. The electrochemical cell consisted of a three-electrode configuration: an Ag/AgCl (sat. KCl) electrode, a Pt plate, and a Au-coated membrane as the reference electrode, the counter electrode, and the working electrode, respectively.

Ni and Fe can be overpotentially electrodeposited as described by Eqs. (1) and (2), respectively.

$$Ni^{2+} + 2e^- \rightarrow Ni\ (s),\ E^0\ (Ni^{2+}/Ni^0) = -0.26\ V\ (vs.\ SHE) \quad (1)$$

$$Fe^{2+} + 2e^- \rightarrow Fe\ (s),\ E^0\ (Fe^{2+}/Fe^0) = -0.41\ V\ (vs.\ SHE) \quad (2)$$

The alternative electrodeposition of the Ni-rich and Fe-rich segments of the NiFe nanowires using the electrolyte can be controlled by varying the relative deposition rate of the electroactive species. In our experiments, alternating Ni-rich and Fe-rich segments were grown by applying two plating current densities alternately to the bath: 5 $mAcm^{-2}$ for the Ni-rich segments and 20 $mAcm^{-2}$ for the Fe-rich segments. The operating temperature and agitation were fixed at 40 °C and 200 rpm, respectively. Composition of the Ni-rich segment was $Ni_{70}Fe_{30}$ and that of Fe-rich segment was $Ni_{21}Fe_{79}$, as was reported previously.[22] The nanowires were suspended by dissolving the templates. The dissolving solution for AAO was 1 M NaOH and that for polycarbonate was 99.5% 1-methyl-2-pyrrolidinone.

Bamboo-like Te nanotubes were produced by employing the GDR process to the sacrificial NiFe nanowires. The GDR electrolyte consisted of 0.01 M TeO_2 dissolved in 1 M HNO_3. The GDR process was carried out by immersing the NiFe nanowires in the electrolyte solution at room temperature for various reaction times: 10 min, 30 min, 60 min, 120 min, and 300 min.

The variations of the open circuit potential (OCP) were determined for the GDRs of Ni-rich and Fe-rich NiFe films in the same electrolyte, and Tafel plots were obtained. The films were electrodeposited on 100 nm thick Au-coated SiO_2/Si wafers with the electrochemical parameters corresponding to those used in the electrodeposition of the NiFe nanowire. The morphologies, crystallinities, and compositions of the synthesized NiFe nanowires and Te nanotubes were investigated by using SEM (XLG-30FEG, Philips), TEM (JEM-2100F, JEOL), and energy dispersive spectroscopy (EDS).

Results and Discussion

Figure 1 shows the morphology of a segmental NiFe nanowire electrodeposited in AAO with a pore size of 200 nm and the EDAX analyses of the segments. The tailored lengths of the bright and dark components of the segmental NiFe nanowire are 568 ± 57 nm and 276 ± 31 nm respectively. The EDAX analyses show that the chemical compositions of the Ni-rich NiFe and Fe-rich NiFe segments are $Ni_{70}Fe_{30}$ and $Ni_{21}Fe_{79}$ respectively.

The prepared sacrificial NiFe nanowires were immersed in an electrolyte containing $HTeO_2^+$ ions in acidic HNO_3 solution to allow the GDR to proceed. The GDRs of both the Ni-rich and Fe-rich segments are driven by the overpotential deposition of Te, which is due to the difference between the redox potentials of the standard reduction potentials of H to TeO_2^+/Te^0 [E^0 = 0.55V (*vs.* SHE)] and the sacrificial materials (*e.g.*, Ni^{2+}/Ni^0 [E^0 = –0.26 V (*vs.* SHE)] and Fe^{2+}/Fe^0 [E^0 = -0.41 V (*vs.* SHE)]), and can be expressed as

$$HTeO_2^+ + 2M\ (s) + 3H^+ \rightarrow Te^0\ (s) + 2M^{2+} + 2H_2O \quad (3)$$

where M is the sacrificial metal, in this case Ni and Fe. The reaction of sacrificial Fe has a more negative reduction potential, –0.41 V (*vs.* SHE), and so is thermodynamically preferred to that of Ni, which has a less negative reduction potential, –0.26 V (*vs.* SHE). A TEM image and an EDAX analysis of the Te nanotubes after 30 min reaction are shown in Figure 2. The bright field image shows that the Te nanotubes have a bamboo-like tube structure. Ni-rich segments of the NiFe wires produced the thick sections (stalks) whereas

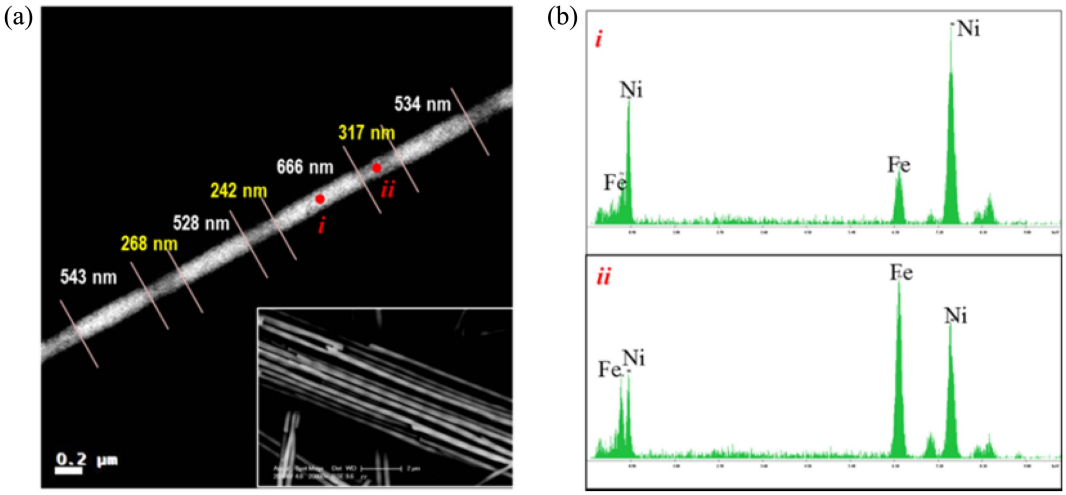

Figure 1. (a) STEM image of a segmental NiFe nanowire (inset: SEM image) and (b) EDAX analyses of a Ni-rich segment (*i*) and a Fe-rich segment (*ii*).

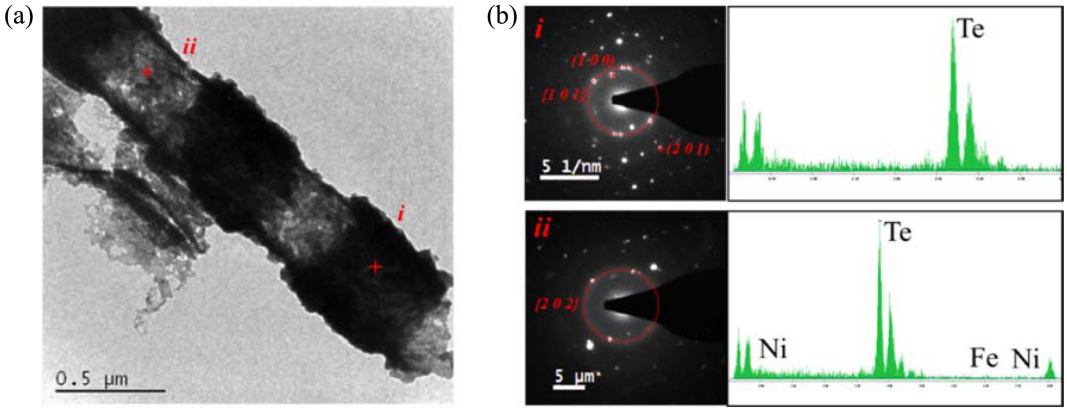

Figure 2. Results for a bamboo-shaped Te nanotube produced by the conversion of segmental NiFe nanowires *via* the galvanic displacement reaction for 30 min: (a) bright field TEM image and (b) SAED patterns/EDAX analyses for the Ni-rich component (*i*) and the Fe-rich component (*ii*).

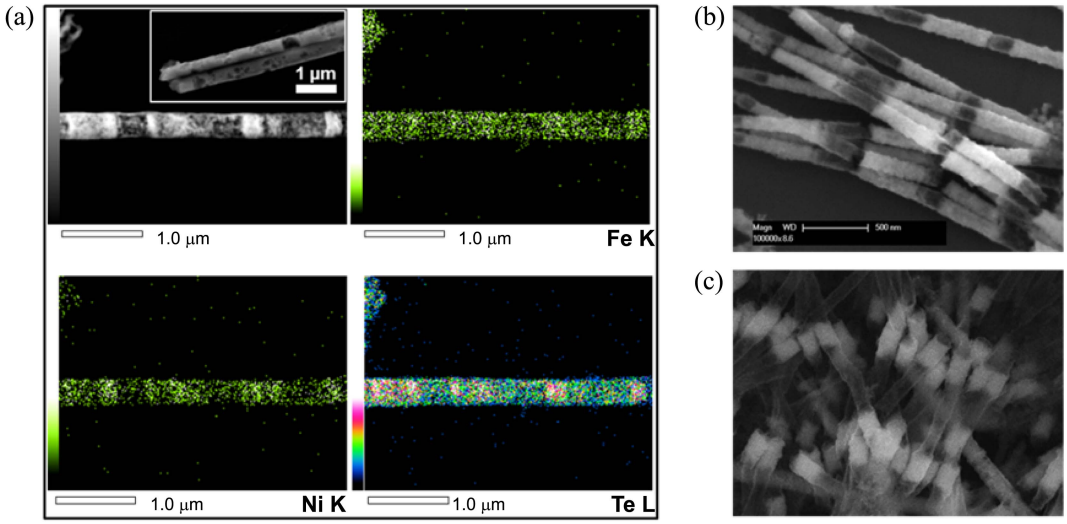

Figure 3. (a) EDAX mapping of the elements Fe, Ni, and Te in the Te nanotubes after 10 min of the displacement reaction (inset: SEM image) and SEM images of Te nanotubes converted from sacrificial NiFe nanowires with modulated segment lengths of (b) 500 nm (Ni-rich segments) and 320 nm (Fe-rich segments) and (c) 320 nm (Ni-rich segments) and 500 nm (Fe-rich segments).

the Fe-rich segments yielded thin sections (nodes) of the Te nanotubes. The selected area electron diffraction (SAED) patterns of the segments are those of polycrystalline Te: {101} planes with a d-spacing of 3.314 Å for a stalk and {202} planes with a d-spacing of 1.689 Å for a node. The EDAX spectrum for a node in the bamboo-like structure is that of Te without residual Ni or Fe peaks while approximately 0.2% Ni and 1% Fe are present in the stalks of Te.

The EDAX mapping in Figure 3(a) shows the levels of the elements Ni, Fe, and Te at the start of the displacement reaction, *i.e.*, after 10 min in the GDR electrolyte. Abundant Ni residue is evident in the stalks of the bamboo-like structures, *i.e.* in the Ni-rich component rather than in the Fe-rich component. In contrast, Fe residue is homogeneously distributed within the Te nanotubes. These results for the Te nanotubes arising from the sacrificial NiFe nanowires with modulated segment lengths also reveal the origins of the stalks and nodes in the bamboo-like Te structures. The segmental NiFe nanowires with 500 nm Ni-rich components and 320 nm Fe-rich components produce Te structures with long stalks and short nodes, and vice versa (Figures 3(b) and (c)). These results indicate that the segment dimensions of the bamboo-like Te nanotubes can be controlled through the modulation of the diameter and segment lengths of the NiFe nanowires.

The evolution of the GDR morphology is shown in Figure 4. The GDR of the segmental NiFe nanowires initially produces a partially porous surface, as shown in the inset in Figure 3(a). Te nanostructures with thick stalks and porous nodes are produced after 30 min by the difference between the reactivities of the Ni-rich and Fe-rich segments in the sacrificial NiFe nanowires. The nodes in the bamboo-like Te structures have distinct tube-like structures after 60 min of reaction. As the reaction proceeds, the walls of the stalks and nodes of the Te nanotubes become thinner and more porous. After 300 min of reaction, the node segments of the Te nanostructures are completely removed, as shown in Figure 4(d).

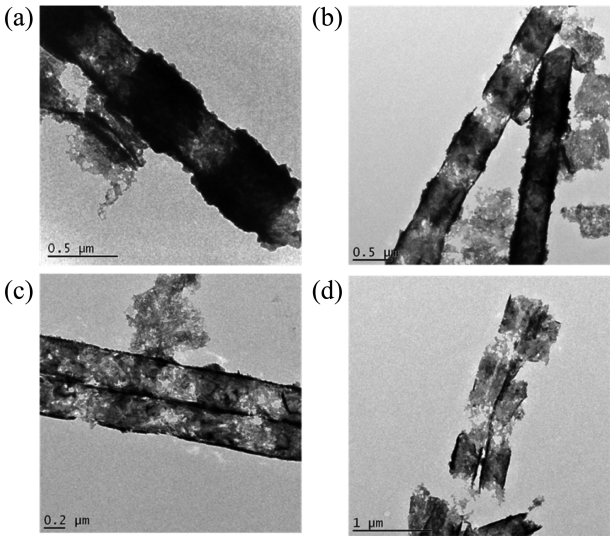

Figure 4. Evolution of the morphology of the Te nanostructures during the GDR: (a) 30 min, (b) 60 min, (c) 120 min, and (d) 300 min.

We consider that the synthesis of bamboo-like Te nanotubes is driven by the difference of the reactivities of the segments. The reactivities of the segments in the sacrificial NiFe nanowires with the electrolyte containing $HTeO_2^+$ ions in acidic solution can be evaluated by performing OCP measurements and Tafel plot analyses for Ni-rich and Fe-rich NiFe films. While the OCP of the Ni-rich NiFe film varies gradually, the OCP of the Fe-rich NiFe film increases very rapidly in approximately 60 s, as can be seen in Figure 5(a). Additionally, the corrosion behaviors of the Ni-rich and Fe-rich NiFe films in the GDR electrolyte were evaluated with Tafel plot analyses, as shown in Figure 5(b). The polarization resistances are 7.65 Ωcm^2 and 6.68 Ωcm^2 for the Ni-rich and Fe-rich NiFe thin films respectively, which indicates that Ni-rich NiFe is less easily corroded in the electrolyte than Fe-rich NiFe.

Our analysis shows that the GDR of the segmental NiFe nanowires in the electrolyte containing $HTeO_2^+$ ions can be depicted as shown in Figure 6. In the case of the GDR of

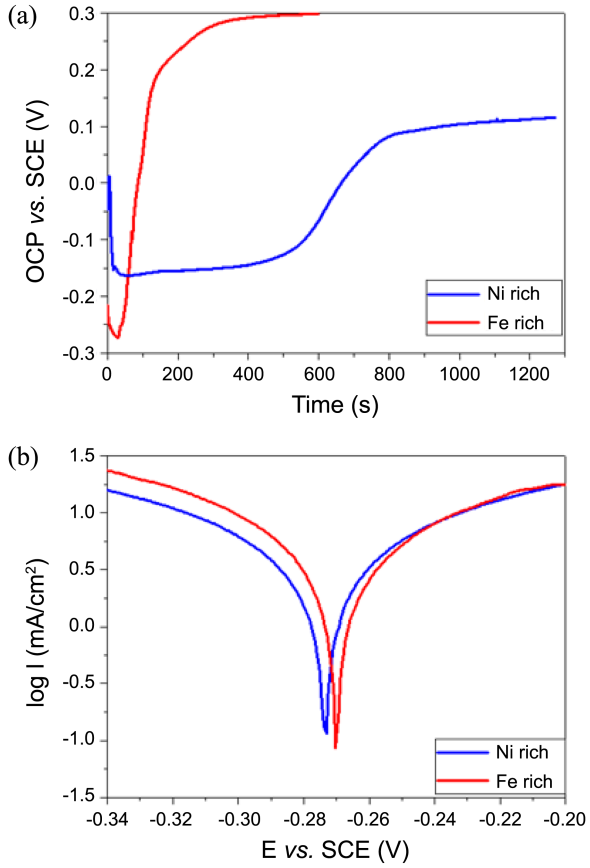

Figure 5. (a) Open circuit potential transients and (b) Tafel plots for Ni-rich and Fe-rich NiFe films in an electrolyte containing 0.01 M TeO_2 and 1 M HNO_3.

Bi_xTe_y, the underpotential deposition of Bi follows the overpotential deposition of Te.[9,22,31] The underpotential-deposited Bi layers are alternately stacked with the overpotential-deposited Te. The GDR of the dissolving sacrificial NiFe occurs only through the overpotential deposition of Te. In contrast to the GDR of Bi_xTe_y, the more reactive Fe-rich NiFe segments are converted to the thinner stalks in the bamboo-like Te nanotubes, not the thicker nodes. This

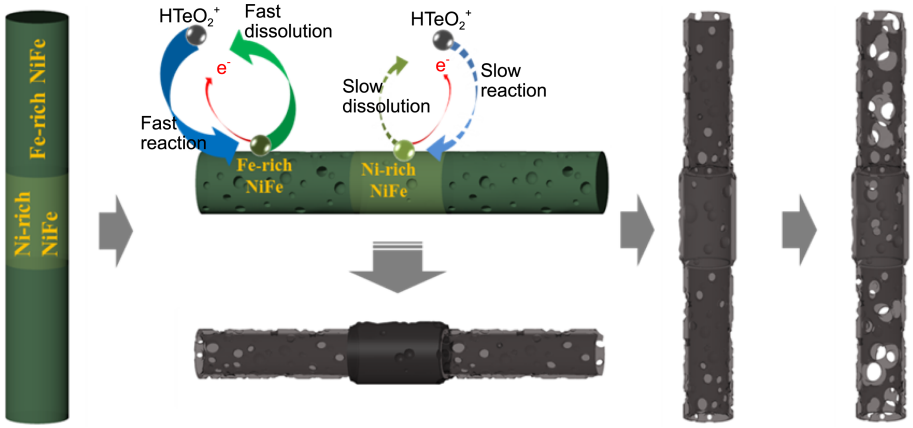

Figure 6. Schematic diagram of the galvanic displacement reaction of a segmental NiFe nanowire with Ni-rich and Fe-rich NiFe segments in an electrolyte consisting of $HTeO_2^+$ ions in acidic HNO_3 solution.

difference might be due to the reaction mechanism of the overpotential deposition, which is not followed by an underpotential deposition. The Fe-rich NiFe segments have higher reactivity and so dissolve as illustrated in Figure 6. The $HTeO_2^+$ ions continue to directly displace the inner sacrificial NiFe without any stacking of underpotential-deposited ions on Te. In contrast to the underpotential deposition of ions with the residues of sacrificial materials when layers stack on the surface, the displaced Te nanotubes do not contain Ni and Fe residues. As a result, the initially displaced Te consists of Te nanotube stalks arising from the more reactive Fe-rich segments and Te nanowire nodes arising from the less reactive Ni-rich segments. As the reaction proceeds, the structures of the nodes become more tube-like and porous, as shown by the transient TEM analysis in Figure 4.

Conclusion

We have demonstrated that the GDR of segmented NiFe nanowires could produce bamboo-like Te nanotubes. The transient OCP of Fe-rich NiFe indicates that it undergoes a kinetically more rapid reaction than Ni-rich NiFe. The Tafel analysis also shows that Fe-rich NiFe is more easily corroded than Ni-rich NiFe. The GDR of segmental NiFe in an electrolyte containing $HTeO_2^+$ ions offers a feasible approach to the synthesis of bamboo-like Te nanotubes *via* the overpotential deposition of Te with different reactivities on the sacrificial NiFe segments. In addition, the segment dimensions of the synthesized bamboo-like Te nanotubes can be modulated by varying the dimensions of the segments in the sacrificial material and the GDR time.

Acknowledgments. This study was supported in part by a National Research Foundation of Korea grant (NRF-2014-004785).

References

1. Yang, P. *MRS Bulletin* **2005**, *30*, 85.
2. Duan, X.; Huang, Y.; Cui, Y.; Wang, J.; Lieber, C. M. *Nature* **2001**, *409*, 66.
3. Cui, Y.; Wei, Q.; Park, H.; Lieber, C. M. *Science* **2001**, *293*, 1289.
4. Pan, Z. W.; Dai, Z. R.; Wang, Z. L. *Science* **2001**, *291*, 1947.
5. Thurn-Albrecht, T.; Schotter, J.; Kastle, G. A.; Emley, N.; Shibauchi, T.; Krusin-Elbaum, L.; Guarini, K.; Black, C. T.; Tuominen, M. T.; Russell, T. P. *Science* **2000**, *290*, 2126.
6. Meng, G.; Han, F.; Zhao, X.; Chen, B.; Yang, D.; Liu, J.; Xu, Q.; Kong, M.; Zhu, X.; Jung, Y. J.; Yang, Y.; Chu, Z.; Ye, M.; Kar, S.; Vajtai, R.; Ajayan, P. M. *Angew. Chem. int. Edit* **2009**, *48*, 7166.
7. Chen, X.; Cui, C.-H.; Guo, Z.; Liu, J.-H.; Huang, X.-J.; Yu, S.-H. *Small* **2011**, *7*, 858.
8. Wang, C.-Y.; Gong, N.-W.; Chen, L.-J. *Adv. Mater.* **2008**, *20*, 4789.
9. Jung, H.; Suh, H.; Hangarter, C. M.; Lim, J. H.; Lee, Y.-I.; Choa, Y.-H.; Hong, K.; Myung, N. V. *Appl. Phys. Lett.* **2012**, *100*, 223105.
10. Hangarter, C. M.; Lee, Y.-I.; Hernandez, S. C.; Choa, Y.-h.; Myung, N. V. *Angew. Chem. int. Edit* **2010**, *49*, 7081.
11. Mohseni, P. K.; Lawson, G.; Adronov, A.; LaPierre, R. R. *IEEE J. Sel. Top. Quant.*, **2011**, *17*, 1070.
12. Chang, P. C.; Fan, Z.; Wang, D.; Tseng, W. Y.; Chiou, W. A.; Hong, J.; Lu, J. G. *Chem. Mater.* **2011**, *16*, 5133.
13. Hao, Y.; Meng, G.; Ye, C.; Zhang, L. *Cryst. Growth. Des.* **2005**, *5*, 1617.
14. Lin, H.-M.; Chen, Y.-L.; Yang, J.; Liu, Y.-C.; Yin, K.-M.; Kai, J.-J.; Chen, F.-R.; Chen, L.-C.; Chen, Y.-F.; Chen, C.-C. *Nano Lett.* **2003**, *3*, 537.
15. Mohanty, P.; Kang, T.; Kim, B.; Park, J. *J. Phys. Chem. B* **2005**, *110*, 791.
16. Wang, Q.; Li, G.-D.; Liu, Y.-L.; Xu, S.; Wang, K.-J.; Chen, J.-S. *J. Phys. Chem. C* **2007**, *111*, 12926.
17. Hawley, C. J.; Beatty, B. R.; Chen, G.; Spanie, J. E. *Cryst. Growth. Des.* **2012**, *12*, 2789.
18. Sun, Y.; Wiley, B.; Li, Z.-Y.; Xia, Y. *J. Am. Chem. Soc.* **2004**, *126*, 9399.
19. Zhang, Y.; Wang, H.; Kraemer, S.; Shi, Y.; Zhang, F.; Snedaker, M.; Ding, K.; Moskovits, M.; Snyder, G. J.; Stucky, G. D. *ACS Nano* **2011**, *5*, 3158.
20. Hormozi Nezhad, M. R.; Aizawa, M.; Porter, L. A.; Ribbe, A. E.; Buriak, J. M. *Small* **2005**, *1*, 1076.
21. Xiao, F.; Yoo, B.; Lee, K. H.; Myung, N. V. *J. Am. Chem. Soc.* **2007**, *129*, 10068.
22. Suh, H.; Jung, H.; Hangarter, C. M.; Park, H.; Lee, Y.; Choa, Y.; Myung, N. V.; Hong, K. *Electrochim. Acta* **2012**, *75*, 201.
23. Elazem, D.; Jung, H.; Wu, T.; Lim, J.-H.; Lee, K.-H.; Myung, N. V. *Electrochim. Acta* **2013**, *106*, 447.
24. Jung, H.; Rheem, Y.; Chartuprayoon, N.; Lim, J.-H.; Lee, K.-H.; Yoo, B.; Lee, K.-J.; Choa, Y.-H.; Wei, P.; Shi, J.; Myung, N. V. *J. Mater. Chem.* **2010**, *20*, 9982.
25. Park, H.; Jung, H.; Zhang, M.; Chang, C. H.; Ndifor-Angwafor, N. G.; Choa, Y.; Myung, N. V. *Nanoscale* **2013**, *5*, 3058.
26. Liu, Z.; Hu, Z.; Liang, J.; Li, S.; Yang, Y.; Peng, S.; Qian, Y. *Langmuir* **2003**, *20*, 214.
27. Mo, M.; Zeng, J.; Liu, X.; Yu, W.; Zhang, S.; Qian, Y. *Adv. Mater.* **2002**, *14*, 1658.
28. Szymczak, J.; Legeai, S.; Diliberto, S.; Migot, S.; Stein, N.; Boulanger, C.; Chatel, G.; Draye, M. *Electrochem. Commun.* **2012**, *24*, 57.
29. Zhu, Y.-J.; Wang, W.-W.; Qi, R.-J.; Hu, X.-L. *Angew. Chem. Int. Edit* **2004**, *43*, 1410.
30. Jeong, D.-B.; Lim, J.-H.; Lee, J.; Park, H.; Zhang, M.; Lee, Y.-I.; Choa, Y.-H.; Myung, N. V. *Electrochim. Acta* **2013**, *111*, 200.
31. Jung, H.; Myung, N. V. *Electrochim. Acta* **2011**, *56*, 5611.